OATAO
Open Archive Toulouse Archive Ouverte

Open Archive Toulouse Archive Ouverte (OATAO)

OATAO is an open access repository that collects the work of Toulouse researchers and makes it freely available over the web where possible

This is an author's version published in: http://oatao.univ-toulouse.fr/25565

Official URL: https://doi.org/10.1021/acsbiomaterials.9b00795

To cite this version:

Forte, Lucia and Sarda, Stéphanie and Torricelli, Paola and Combes, Christèle and Brouillet, Fabien and Marsan, Olivier and Salamanna, Francesca and Fini, Milena and Boanini, Elisa and Bigi, Adriana *Multifunctionalization Modulates Hydroxyapatite Surface Interaction with Bisphosphonate: Antiosteoporotic and Antioxidative Stress Materials.* (2019) ACS Biomaterials Science & Engineering, 5 (7). 3429-3439. ISSN 2373-9878

Any correspondence concerning this service should be sent to the repository administrator: tech-oatao@listes-diff.inp-toulouse.fr

Multifunctionalization Modulates Hydroxyapatite Surface Interaction with Bisphosphonate: Antiosteoporotic and Antioxidative Stress Materials

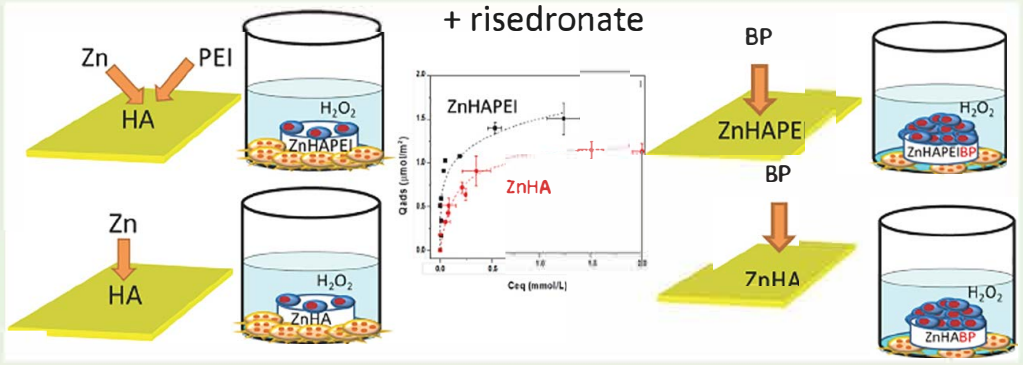
Lucia Forte,[†] Stéphanie Sarda,[‡] Paola Torricelli,[§] Christèle Combes,[‡] Fabien Brouillet,[∥] Olivier Marsan,[‡] Francesca Salamanna,[§] Milena Fini,[§] Elisa Boanini,*[,†] and Adriana Bigi[†]

[†]Department of Chemistry "G. Ciamician", University of Bologna, via Selmi 2, 40126 Bologna, Italy

[‡]CIRIMAT, Université de Toulouse, CNRS, Université Toulouse 3 Paul Sabatier, Toulouse INP ENSIACET, 4 allée Emile Monso, 31030 Toulouse cedex 4, France

[§]Laboratory of Preclinical and Surgical Studies, IRCCS Rizzoli Orthopaedic Institute, via di Barbiano 1/10 40136 Bologna, Italy

[∥]CIRIMAT, Université de Toulouse, CNRS, Université Toulouse 3 Paul Sabatier, Faculté des Sciences Pharmaceutique, 35 Chemin des Maraichers, 31062 Toulouse cedex 9, France



ABSTRACT: Multifunctionalized biomaterials with enhanced bone antiresorptive properties were obtained through adsorption of a bisphosphonate, risedronate, on hydroxyapatite (HA) nanocrystals functionalized with zinc ions and polyethylenimine (PEI). Zn incorporation into the HA structure amounts to about 8 atom %, whereas the PEI content of the bifunctionalized material ZnHAPEIBP is about 5.9 wt %. The mechanism of adsorption and release of the bisphosphonate on ZnHAPEI is compared with that on ZnHA: risedronate adsorption isotherm on ZnHA is a Langmuir type, whereas the isotherm of adsorption on ZnHAPEI is better fitted with a Freundlich model and involved a higher amount of adsorbed risedronate. In vitro cell tests were carried out with a coculture model of osteoblasts and osteoclasts using a model simulating oxidative stress and consequent cellular senescence and osteoporosis by the addition of H_2O_2. The conditions utilized in the coculture model strongly affect osteoblast behavior. The results show that the composite materials allow an increase in osteoblast viability and recover impairment, revealing a novel characteristic of risedronate that is able to counteract the negative effects of oxidative stress when associated with differently functionalized samples. Both PEI and the bisphosphonate reduce osteoclast viability. Moreover, PEI, and even more risedronate, exerts an inhibitory effect on osteoclast activity.

KEYWORDS: *hydroxyapatite, zinc, bisphosphonate, polyethylenimine, adsorption, oxidative stress, osteoporosis*

INTRODUCTION

Bone tissue is a composite material where the inorganic phase is embedded in an organic matrix, mainly constituted of type I collagen.[1] The inorganic phase is a calcium phosphate which is described as a nonstoichiometric hydroxyapatite (HA), characterized by small crystal dimensions and a low degree of crystallinity.[2,3] Because of their similarity to the inorganic phase of bone, synthetic calcium phosphates (CaPs), and in particular HA, are widely employed for the preparation of biomaterials aimed to treat disorders of the musculoskeletal system. Functionalization with biologically active ions, molecules, and drugs can greatly improve the biological performance of CaPs based materials and opens new possible applications in the biomedical field.[4,5] In particular, CaPs have been proposed as delivery systems for the local release of bisphosphonates (BPs).[6,7] Bisphosphonates include several

DOI: 10.1021/acsbiomaterials.9b00795

molecules sharing a common backbone structure, where a carbon atom bonds two phosphonate groups and differing in the two side chains which complete the tetravalence of carbon. These drugs are usefully employed for the treatment of pathologies associated with abnormally high bone resorption, including osteoporosis, Paget's disease, multiple myeloma, and bone metastases.[6−10] However, BPs display several negative characteristics, such as low bioavailability, and important side effects due of oversuppression of bone resorption,[11] including osteonecrosis of the jaw and atypical subtrochanteric femoral fractures.[10,12−14] The use of CaPs, as well as of other materials, as delivery systems for BPs has been proposed as a strategy to provide local administration of these drugs and reduce the doses of systemic administration and related side effects.[10,11] The binding affinity of BPs to hydroxyapatite depends on the chemistry of their side chains.[15] On the other hand, the structure and chemistry of the apatitic surface influence the parameters of adsorption of BPs, and their release kinetics as the main reaction is an ion exchange process (chemisorption) between BPs in solution and phosphate ions on the apatite crystal surface.[16−19] Previous papers show that higher amounts of BPs were adsorbed on nanocrystalline apatites (NCA) compared to well crystalline stoichiometric HA, which has been explained by the NCA surface composition rich in labile species able to be exchanged and the higher specific surface area of the nanocrystals. Similarly, the maturation time of NCA influences the development of the surface hydrated layer and its composition: immature apatitic samples exhibit higher amounts of BPs both adsorbed and released compared with matured apatitic crystals.[18] We have previously shown that a partial substitution of the Zn^{2+} ion to the Ca^{2+} ion into the HA structure provokes just minor variations in the mechanisms of adsorption (chemisorption) and release of the risedronate.[19] On the other hand, functionalization of HA with a cationic polymer, polyethylenimine (PEI), modifies the interactions with risedronate, so that its adsorption implies not just chemisorption but also physisorption, which also influences its release.[19] The structures of risedronate and of PEI are reported in Supporting Information (Scheme S1). Zinc substituted hydroxyapatite was shown to inhibit osteoclast proliferation and activity.[20] Similarly, zinc substituted tricalcium phosphate was reported to reduce osteoclast number and activity in vitro.[21] Moreover, zinc containing calcium phosphates pos itively influence osteoblast response: the presence of zinc in the apatite layer deposited on Ti external fixation rods increased osteoblast proliferation and differentiation in vitro.[22] Furthermore, a zinc containing calcium phosphate cement implanted in the femora and tibia of rabbits was shown to promote new bone formation around the implants.[23] In the present work, we developed multifunctionalized materials able to add the downregulating effect of zinc on osteoclastogenesis and osteoclast activity to the antiresorptive properties of risedronate.[20−25] To this aim, Zn substituted hydroxyapatite was functionalized with PEI (ZnHAPEI). The double functionalization should increase the amount of adsorbed risedronate, thanks to the presence of the polycationic polymer on the surface of the crystals of the composite material. The influence of PEI on the adsorption and release mechanisms of risedronate on/from ZnHAPEI was evaluated by comparing the results with those obtained on zinc substituted hydrox yapatite (ZnHA). Coculture systems with osteoblasts and osteoclasts, are a useful in vitro model for biomaterial testing, as they mimic the human physiological microenvironment in the complex process of bone formation and resorption. As the functionalized biomaterials should affect both osteoblast and osteoclast behavior, bone cells' response to the materials with and without adsorbed risedronate was tested in vitro using a coculture model of osteoblast (OB) and osteoclast (OC) added with hydrogen peroxide (H_2O_2), in order to increase the generation of reactive oxygen species (ROS) and simulate in vitro the condition of cellular senescence and osteoporosis.

MATERIALS AND METHODS

Synthesis of the Apatitic Samples. The synthesis of zinc substituted hydroxyapatite (ZnHA) was carried out in N_2 atmosphere using CO_2 free distilled water.[19] A total of 50 mL of a solution containing $Ca(NO_3)_2{\cdot}4H_2O$ and $Zn(NO_3)_2{\cdot}6H_2O$ with 1.08 M total cationic concentration, and a Zn/(Ca + Zn) molar ratio of 0.1 (pH adjusted to 10 with NH_4OH) was heated at 90 °C. Dropwise addition of 50 mL of 0.65 M $(NH_4)_2HPO_4$ solution under stirring led to the fast formation of a precipitate, which was separated from the reaction solution after 5 h of maturation at 90 °C under stirring through centrifugation at 10 000 rpm for 10 min. Then, the solid product was repeatedly washed with CO_2 free distilled water and dried at 37 °C overnight.

Adsorption of polyethylenimine (PEI, Sigma, MW ≅ 2000 g mol^{-1}) on the as prepared ZnHA was performed by soaking ZnHA powder (100 mg) in an aqueous solution of 4 M PEI, under stirring for 24 h. Then, the solid was centrifuged at 10 000 rpm for 10 min and washed with deionized water. Finally, the powder was dried at 37 °C, and the sample was labeled as ZnHAPEI.

Risedronate Adsorption and Release. Adsorption experiments were carried out in triplicate on ZnHA and ZnHAPEI by dispersing 50 mg of powder in 5 mL of adsorption medium, an aqueous solution of risedronate (Aldrich, from 0 to 3 mM in 1 mM KCl solution at physiological pH 7.4 adjusted by addition of HCl or KOH solution) in a polyethylene tube. After sonication for 1 min, the suspensions were incubated for 1 h at physiological temperature (37 ± 1 °C) without stirring. After centrifugation for 10 min at 5000 rpm, the supernatants obtained were filtrated onto 0.2 μm Millipore filters, and these solutions were stored in a refrigerator at 4 °C before titration. The solids were washed with deionized water and dried at 37 °C overnight before their characterization. The solids at maximum risedronate content reached in this work (1.2 and 1.5 $\mu mol/m^2$ for ZnHA and ZnHAPEI respectively) were labeled ZnHABP and ZnHAPEIBP.

The supernatants after adsorption were analyzed for risedronate and phosphate content. Risedronate concentration was determined by UV spectrophotometric absorption at 262 nm (Hewlett Packard 8452A diode array spectrophotometer), corresponding to the maximum absorbance of the pyridine group of the risedronate molecule. Phosphorus concentration was determined by inductively coupled plasma atomic emission spectroscopy (ICP AES, Horiba Jobin Yvon).

The release profiles of risedronate were recorded using a flowthrough cell system (USP Apparatus 4 Sotax CE6, Sotax AG, Switzerland) with 12 mm cells for powders and a peristaltic pump. In all experiments, laminar flow was used with one glass beads layer covered with each sample, mixed with 2 g of glass beads. The analyses were performed utilizing different quantities of the tested materials so that the amount of adsorbed BP was the same (about 1.8 μmol) in all the examined samples, ZnHA and ZnHAPEI. The European Pharmacopeia guidelines were followed for the release tests, which were performed at 37.0 ± 0.5 °C under sink conditions using deionized water pumped through the column at a flow rate of 9 mL/min. A closed system was used, recycling 50 mL of release medium. Periodically, fractions of 5 mL were collected for determination of risedronate content by UV spectrophotometry at 262 nm. After each sampling, the same volume of release medium was replaced back in the cell system. Each release test was performed in triplicate. The results are presented as cumulated BP release (%) profiles as a function of time.

Solid Samples Characterization. Elemental analyses were performed by means of an inductively coupled plasma (ICP) mass spectrometer (ICP AES, Horiba Jobin Yvon) on powders previously dissolved in 0.6 M HNO_3 solution.

X ray diffraction analysis was carried out by means of a PANalytical X'Pert PRO powder diffractometer equipped with a fast X'Celerator detector. Cu Kα radiation was used (40 mA, 40 kV). The 2θ range was from 10° to 60° with a step size of 0.1° and time/step of 100 s. The lattice parameters were determined by least squares refinements from the well determined positions of the most intense reflections using the HighScore Plus software package (PANalytical). The peak broadening was used to evaluate the crystal size (τ_{hkl}), which was calculated from the width at half maximum intensity ($\beta_{1/2}$) using the Scherrer equation:

$$\tau_{hkl} = \frac{K\lambda}{\beta_{1/2}\cos\theta} \quad (1)$$

where λ is the wavelength, θ the diffraction angle, and K a constant depending on crystal habit (chosen as 0.9).

Morphological investigation was performed using a Philips CM100 transmission electron microscope, operating at 80 kV. A drop of sonicated sample suspension in ethanol was transferred onto Formvar films supported on conventional copper microgrids.

Thermogravimetric analysis was performed by means of a PerkinElmer TGA 7. Samples (5−10 mg) were examined in a platinum crucible in air flow (20 cm^3/min) at a rate of 10 °C/min up to 800 °C. Results represent the mean value of weight losses measured for three different samples.

Zeta potential was measured using a Malvern Instruments Zetasizer Nano. For the analysis, which was performed in triplicate, 5 mg of powder sample was suspended in 50 mL of Milli Q water and sonicated for 2 min.

The specific surface area was measured using a Carlo Erba Sorpty 1750 BET analyzer using constant volume N_2 adsorption with desorption at 80 °C.

Raman spectroscopy was performed using a Horiba, Jobin Yvon Labram HR800 confocal microspectrometer with a helium−neon laser (632.82 nm) over a wavelength range of 400−4000 cm^{-1}. The spectral resolution was 2 cm^{-1}, the laser power was 2 mW, and integration times varied from 30 to 120 s. Three spectral accumulations were averaged.

In Vitro Coculture Model. In vitro tests were carried out on disk shaped samples (Ø = 6.0 mm). Each disk was prepared by pressing 40 mg of powder into cylindrical molds by using a standard evacuable pellet die (Hellma).

AFM analysis of the disk shaped samples was performed using a Veeco Nanoscope 3D instrument. The samples were analyzed in tapping mode using an E scanner (maximum scan size 15 μm) and phosphorus (n) doped silicon probes (spring constant 20−80 N/m; resonance frequency 250−290 kHz; nominal tip radius < 10 nm).

Before in vitro tests, the samples were sterilized using γ rays (Cobalt 60) at a dose of 25 kGy.

In Vitro Oxidative Stress Coculture Model. Human osteoblast like cells MG63 (OB, Istituto Zooprofilattico Sperimentale IZSBS, Brescia, Italy) and human osteoclast precursor 2T 110 (OC, Poietics Osteoclast Precursor Cell System, Lonza Walkersville, Inc., MD, USA) were used for the coculture model.

The coculture model was set up according to the following indications: preosteoclasts were plated at a concentration of 3×10^4 cells/well in the bottom of 24 well plates leaving a little central empty space. They were fed for 7 days with DMEM additioned with macrophage colony stimulating factor (MCSF, 25 ng/mL) and receptor activator for κB factor ligand (RANKL, 30 ng/mL) in standard condition, at 37 ± 0.5 °C with 95% humidity and 5 ± 0.2% CO_2 to activate cell differentiation. In the meantime, osteoblasts were expanded in DMEM supplemented with 10% FCS, 1% antibiotics (100 U/mL penicillin, 100 μg/mL streptomycin), β glycerophosphate (10^{-4} M), and ascorbic acid (50 μg/mL). After 6 days, OB were counted, seeded at a concentration of 2×10^4 cells/well onto biomaterial samples (ZnHA, ZnHAPEI, ZnHABP, ZnHAPEIBP) in their own differentiation medium (DMEM supplemented with 10% FCS, 1% antibiotics (100 U/mL penicillin, 100 μg/mL streptomycin), β glycerophosphate (10^{-4} M), and ascorbic acid (50 μg/mL)) and allowed to adhere for 24 h. Then, samples seeded with osteoblasts were placed in the empty space of the well containing differentiating osteoclasts (Scheme S2). When cells were cultured together, a mix of medium was used, according to cell concentration proportion.

Cocultures with materials (ZnHA+, ZnHAPEI+, ZnHABP+, ZnHAPEIBP+) were treated with 0.3 mM H_2O_2 for 48 h. The ZnHA group was not treated with H_2O_2 and was used as a reference. After 48 h, the medium was renewed with fresh medium without H_2O_2 in all cultures that were maintained in standard conditions up to 7 days.

Cell Viability and Morphology. To assess viability of OB and OC separately, cocultures were disassembled, and material samples with OB were transferred to empty wells. WST1 colorimetric reagent test (Roche Diagnostics GmbH, Manheim, Germany) was performed at 3 and 7 days of coculture. The assay is based on the reduction of tetrazolium salt to a soluble formazan salt by a reductase of the mitochondrial respiratory chain, active only in viable cells. A total of 100 μL of WST1 solution and 900 μL of medium (final dilution: 1:10) were added to wells containing OC or materials with OB, and the multiwell plates were incubated at 37 °C for the next 4 h. Supernatants were quantified spectrophotometrically at 450 nm with a reference wavelength of 625 nm. Results of WST1 are reported as optical density (OD) and directly correlated with the cell number.

Random material samples of all groups were stained with the Live/Dead assay (Molecular Probes, Eugene, OR, USA), according to the manufacturer's instructions to detect osteoblast colonization of samples. Samples were visualized using an inverted microscope equipped with an epifluorescence setup (Eclipse TiU, NIKON Europe BV, NITAL SpA, Milan, Italy): excitation/emission setting of 488/530 nm to detect green fluorescence (live cells) and 530/580 nm to detect red fluorescence (dead cells).

Tartrate resistant acid phosphatase (TRAP) staining was performed to assess osteoclast differentiation starting from mono nucleated cells, according to manufacturer's instructions (Sigma, Buchs, Switzerland). The positive cells are multinucleated cells (three or more nuclei for each cell) and developed red color of different intensities. Osteoclastogenesis was evaluated by counting the number of TRAP positive cells, under the microscope by a semiautomatic software (NIS Elements AR 4.30.01). Results are given as the percentage of differentiated OC considering ZnHA− as reference (100%).

Immunoenzymatic Assay. At the end of experimental time, the supernatant was collected from all wells and centrifuged to remove particulates, if any. Aliquots of supernatant were dispensed in Eppendorf tubes for storage at −70 °C and assayed with the following immunoenzymatic kits: alkaline phosphatase (ALP), CloudClone Corp., Wuhan, China), collagen type I (COLL1, CloudClone), osteoprotegerin (OPG, CloudClone), receptor activa tor for nuclear factor KB ligand (RANKL, CloudClone).

qPCR. Total RNA was extracted from all samples at the end of experimental time using the PureLink RNA mini kit (Life Technologies, Carlsbad, CA, USA). Purified RNA was reverse transcribed with the Superscript VILO cDNA synthesis kit (Invitrogen, Life Technologies, Carlsbad, CA, USA), following manufacturer's instructions. Each sample (10 ng) was tested in duplicate. qPCR analysis was performed in a LightCycler instrument (Roche Diagnostics GmbH, Mannheim, Germany) using the QuantiTect SYBR Green PCR kit (Qiagen, Hilden, Germany). The protocol included a denaturation at 95 °C for 15 s, 40 cycles of amplification (95 °C for 15 s, appropriate annealing temperature for each target as detailed in Table S1 for 20 s, a final extension at 72 °C for 20 s), and a melting curve to check for amplicon specificity. The threshold cycle was used for the calculation of relative expression by means of the 2 ΔΔCt method against GAPDH as the reference gene, and ZnHA− samples as the calibrator. Studied genes are summarized in Table S1.

Statistical Analysis. Statistical evaluation of in vitro biological tests data was performed using the software package SPSS/PC$^+$ Statistics 23.0 (SPSS Inc., Chicago, IL USA). The results presented are the mean of six independent values. Data are reported as mean ± standard deviation (SD) at a significance level of $p < 0.05$. After normal distribution and homogeneity of variance were verified, a one way ANOVA was done for comparison between groups, and a post hoc multiple comparison test was performed to detect significant differences among groups for the ELISA test and qPCR.

RESULTS AND DISCUSSION

Characterization of the As-Prepared Supports. The X ray diffraction pattern of ZnHA shows a number of reflections which indicate the presence of a unique crystalline apatitic phase (Figure 1). The reduced values of the calculated lattice constants (Table 1) in comparison to those of pure HA synthesized with the same procedure (a = 9.4378(3) Å, c = 6.8862(2) Å) are in agreement with a partial substitution of the smaller zinc ion (ionic radius = 0.074 nm) to the calcium ion (ionic radius = 0.099 nm) in the hydroxyapatite structure.[26] Zn incorporation amounts to about 8 atom %, as determined by ICP analysis and provokes a slight broadening of the diffraction peaks that hinders the complete resolution of the characteristic three peaks of HA centered at about 32° of 2θ, as well as of further peaks.

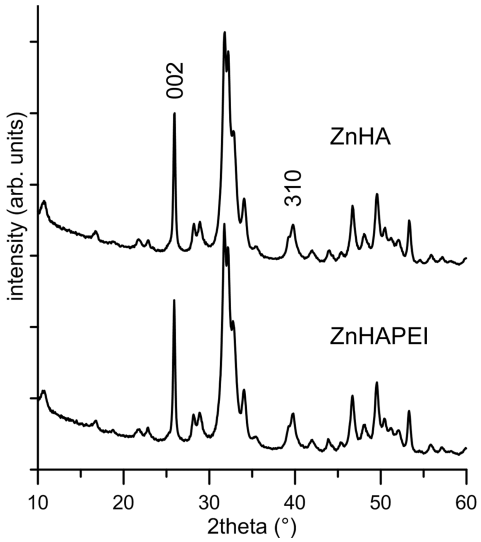


Figure 1. Powder X ray diffraction patterns of as prepared apatitic supports.

The line broadening of the (002) and (310) peaks was used to evaluate the size of the coherently scattering domains (τ_{hkl}) as derived from the Scherrer equation, on the hypothesis of negligible microstrains. The results are reported in Table 1, where τ_{002} is related to the mean crystallite size along the c axis, whereas τ_{310} refers to the mean crystallite size along a direction perpendicular to it. In agreement with previous results, the values are significantly smaller than those reported for HA in the literature and support the known inhibitory role of zinc on hydroxyapatite crystal growth.[19,27,28]

ZnHAPEI was obtained by the immersion of as prepared ZnHA nanocrystals into a PEI solution. To this aim, we used low molecular weight PEI, which was previously shown not to give any osteoblast cytotoxic reaction.[29,30] PEI content of ZnHAPEI is 5.9 wt %, as determined through thermogravi metric analysis from the weight loss centered at about 400 °C of the thermogravimetric plot and due to PEI combustion (Figure S1). PEI adsorption does not significantly affect the structural parameters of the inorganic phase: in agreement with the similar X ray diffraction patterns (Figure 1), both the values of the lattice constants and of the size of coherently scattering domains of ZnHAPEI are close to those of ZnHA (Table 1). Moreover, PEI does not modify the morphology and the specific surface area of the apatitic crystals (Figure S2, Table 1). These results are not surprising in view of the low molecular weight of PEI and of the procedure utilized to functionalize the apatitic crystals with the polymer. In fact, PEI was not introduced into ZnHA synthesis protocol, but it was adsorbed on presynthesized crystals, mostly on their surface. The adsorbed PEI is distributed on a relatively high specific surface area (Table 1), which is not significantly affected by the presence of the low molecular weight polymer. In agreement, previously reported data showed that adsorption of a polymer with a similar low molecular weight did not modify the surface of calcium phosphate crystals, at variance with that observed for the high molecular weight polymer.[31] On the other hand, the presence of the polycationic polymer on the surface of the ZnHAPEI crystals significantly modifies the zeta potential which assumes a positive and significantly high value (Table 1).

Raman spectra of ZnHA and ZnHAPEI (Figure S3) show the ν_1 (960 cm^{-1}), ν_2 (430−460 cm^{-1}), ν_3 (1030−1080 cm^{-1}), and ν_4 (580−610 cm^{-1}) characteristic bands of the apatitic phosphate groups, and the vibration of the apatitic OH band at 3571 cm^{-1}.[32] Whereas the apatitic vibrations are not affected by the presence of PEI on the mineral surface, changes are observed for the organic vibration bands in the Raman spectrum. Slight shifts are detected in the domain of CH_2 wagging and twisting motions especially at 1306 cm^{-1}. The asymmetric (ν_{as}) and symmetric (ν_s) C−H stretching vibration bands, which appear at 2935 and 2866 cm^{-1} for the standard PEI, are shifted downward and upward respectively for ZnHAPEI sample, suggesting a conformational change of the polymer when adsorbed on the apatitic surface.[33] Moreover, the decrease of the ν_s/ν_{as} intensity ratio can be related to the order/disorder character of a polyethylene chain.[33]

Risedronate Adsorption Experiments. The adsorption isotherms of risedronate on Zn substituted hydroxyapatite (ZnHA) and PEI modified Zn substituted hydroxyapatite (ZnHAPEI) at pH 7.4 and 37 °C are presented in Figure 2; they represent the evolution of the amount of risedronate adsorbed on the solids, Q_{ads} (μmol/m^2), as a function of the BP equilibrium concentration in solution, C_{eq}. In agreement

Table 1. Lattice Parameters, Coherent Lengths (τ_{hkl}) of the Perfect Crystalline Domains in the Direction Normal to (002) and to (310), Planes Specific Surface Area (SSA), Zeta Potential, PEI, and Zn Contents of the Different Apatitic Supports

	a (Å)	c (Å)	τ_{002} (Å)	τ_{310} (Å)	SSA (m^2/g)	zeta potential (mV)	PEI content (wt %)	Zn content (atom %)
ZnHA	9.4241(9)	6.8696(2)	367(4)	148(3)	86	15.3		7.9
ZnHAPEI	9.4238(5)	6.8691(4)	365(5)	152(4)	86	+30.9	5.9	7.9

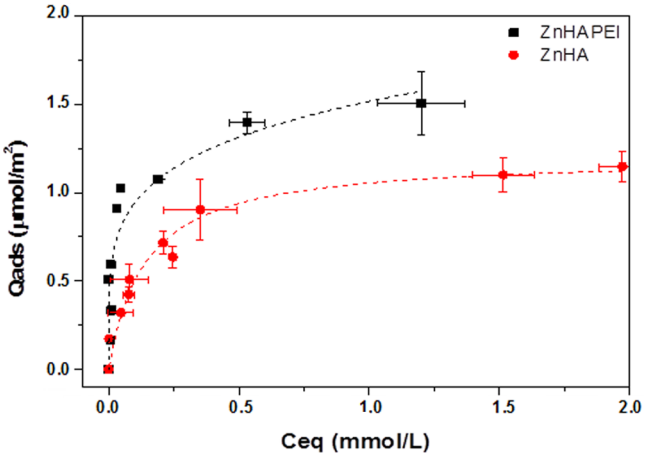


Figure 2. Adsorption isotherms of risedronate on Zn substituted hydroxyapatite (ZnHA) and PEI modified Zn substituted hydroxyapatite (ZnHAPEI) at pH 7.4 and 37 °C. The ZnHA and ZnHAPEI data are fitted with a Langmuir and a Freundlich isotherm, respectively.

with previous data,[19] the isotherm obtained for ZnHA is a Langmuirian type (r^2 = 0.94).

The plateau was reached at relatively low equilibrium concentrations of BP (below 1 mM), indicating a high affinity of risedronate for these apatitic surfaces, as observed in the literature for the adsorption of bisphosphonate molecules on various apatitic supports.[18] The parameters of adsorption can be determined from the Langmuir equation for ZnHA: the maximum amount of adsorbed risedronate N and the affinity constant of risedronate for the solid surface K are equal to 1.20 ± 0.08 μmol/m^2 and 7 ± 1 L/mmol, respectively.

For ZnHAPEI mineral organic support, the amount of BP molecules adsorbed was higher than on ZnHA, but the curve does not reach a plateau even at a high equilibrium concentration of BP in solution. The isotherm of risedronate adsorption on ZnHAPEI cannot be described by the Langmuir model (as the curve fitting with Langmuir equation model gives a low adjusted correlation coefficient, r^2 = 0.73, and a high standard error for the affinity constant K) but is better fitted with the Freundlich model (r^2 = 0.81):

$$Q_{ads} = KC_{eq}^{\ n} \quad (2)$$

where n and K are the Freundlich constants; the values of n and K obtained for ZnHAPEI support are close to 0.21 ± 0.04 and 1.5 ± 0.2 μmol/m^2, respectively. Freundlich model was also found in the literature to well describe the adsorption of organic molecules, such as uric acid, for example, on PEI composites.[34] Freundlich model is based on several assumptions, including nonequivalent adsorption sites and low interaction adsorbate/surface.

The variation of phosphate ions (PO_4^{3-}) concentration released in solution from the different apatitic supports during adsorption is presented in Figure 3a as a function of adsorbed risedronate amount. For ZnHA support, the amount of phosphate ions released in solution increased linearly as a function of the amount of adsorbed BP. We can observe that the increase of released phosphate from ZnHAPEI support during adsorption of BP is much less significant, and the amount of released phosphate in solution remained low (about 0.5 mM) and appears not to be correlated with the amount of

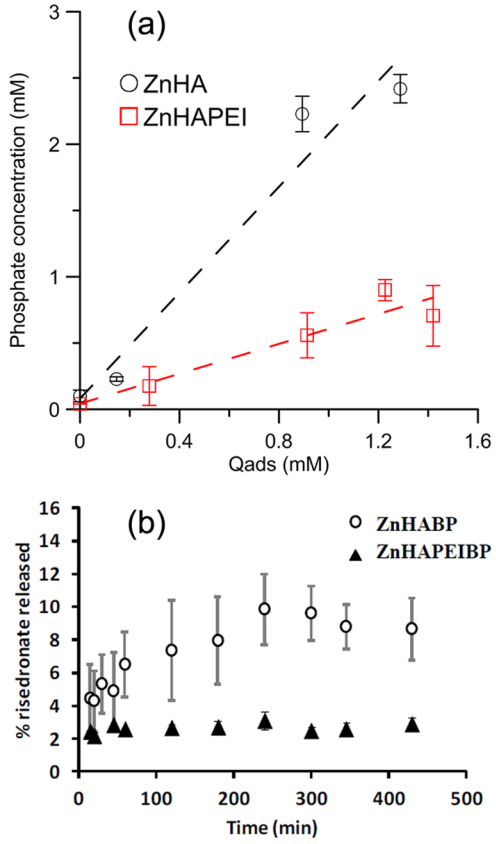


Figure 3. (a) Concentration of phosphate ions released in solution after BP adsorption as a function of the concentration of risedronate adsorbed on the powders, ZnHA and ZnHAPEI (1 mM KCl aqueous solution at pH 7.4 and 37 °C). (b) Risedronate released (wt %) from ZnHABP and ZnHAPEIBP supports as a function of time.

adsorbed risedronate, suggesting different mechanisms of adsorption for these two functionalized apatitic supports.

The low release of phosphate ions is probably mainly due to the slight dissolution of the apatitic substrate during the release experiment. The mechanism of chemisorption by ion exchange process between phosphate groups of the apatitic surface and bisphosphonate in solution, described in many studies for the adsorption of biomolecules or drugs such as bisphosphonates on apatitic supports,[17,18] seemed not relevant for this mineral organic ZnHAPEI support. It suggests the contribution of another mechanism in the case of such PEI functionalized apatitic support, especially physisorption associated with the presence of PEI coating on this composite support. The contribution of chemisorption on apatitic surface and physisorption on PEI coating resulted in a greater BP adsorption content compared with ZnHA mineral support for all the points of the isotherm (Figure 2).

The slight dissolution of the supports during the adsorption experiments is confirmed by the small amounts of calcium and zinc ions measured in the supernatants after BP adsorption: the concentrations of both cations were less than 0.5 mM for ZnHA and less than 2 mM for ZnHAPEI.

Characterization of the Materials after Risedronate Uptake. The comparison of TEM images of ZnHABP and ZnHAPEIBP with those of ZnHA and ZnHAPEI reported in Figure 4 shows that the morphologies of the substrates after risedronate adsorption are not significantly different from those of the as prepared apatitic samples. In agreement, the

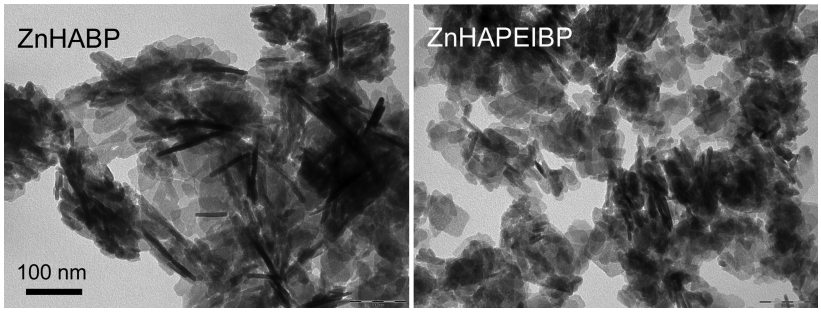


Figure 4. TEM images of the supports after (ZnHABP and ZnHAPEIBP) risedronate adsorption. Magnification in all TEM images is the same for direct comparison.

adsorption of risedronate does not provoke any modification in the value of the specific surface area.

The results of XRD analysis also indicate that the adsorption of risedronate does not alter the crystallinity of the apatitic samples and does not provoke precipitation of any other crystalline phase (Figure S4). ZnHAPEIBP displays a slightly reduced value of zeta potential in comparison to ZnHAPEI (+27.6 mV vs +30.9 mV, respectively), in agreement with the negative charge of risedronate, which interacts with the polycationic polymer. At variance, the value of zeta potential of ZnHA is negative (Table 1) and does not change significantly after risedronate adsorption in ZnHABP (−15.0 mV for ZnHABP vs −15.3 mV for ZnHA).

After adsorption of risedronate, Raman spectra of ZnHABP and ZnHAPEIBP display additional bands characteristic of the presence of BP: pyridine and phosphonate groups vibration bands are observed, as shown in Figure S5 for ZnHABP. However, ZnHABP Raman spectrum shows some changes in the vibration domains of the characteristic bands of BP compared to those of risedronate sodium salt: especially, broadening and shift of the phosphonate vibration bands at 802 and 863 cm^{-1}, the pyridine ring vibration bands (3000−3100 cm^{-1}), and also ν(C−H) stretching (2900−3000 cm^{-1}), ν(C═N) and ν(C═C) stretching (1450 and 1600 cm^{-1}).[35]

As no additional phase has been observed by XRD and TEM observations, these Raman spectroscopy results suggest a strong interaction between BP and calcium on the apatitic surface, in accordance with the Langmuir model proposed for the adsorption process on ZnHA. Similar shifts of the characteristic bands of risedronate are also observed in Raman spectrum of ZnHAPEIBP compared with the BP free molecule (data not shown), with very small differences compared with the ZnHABP spectrum. No difference was observed for the position and intensity of the vibration bands of the PEI macromolecule on ZnHAPEI and ZnHAPEIBP spectra, indicating that PEI was still on the HA surface after BP adsorption experiments and can participate in the process of adsorption of BP.

BP Release Experiments. The kinetics of risedronate release from the different apatitic supports are presented in Figure 3b. For all the samples, the quantity of released risedronate represents a small percentage of the initial adsorbed amount, in accordance with the results observed in the literature for BPs released from apatitic supports.[18] The total amount of risedronate released was higher from ZnHABP (about 9%) than from ZnHAPEIBP (about 3%).

The release from ZnHABP support was fast during the first hour and then slowed down. Therefore, it cannot be described by a simple Higuchi diffusion model (r^2 = 0.83 for ZnHABP),[36] due also to the partial dissolution of the apatitic support occurring at the same time.[18,19] Risedronate molecules were irreversibly adsorbed by an ion exchange process on the apatite supports, and the adsorbed species cannot be removed from the apatitic surface by simple dilution or washing of the solids, as previously demonstrated for biomolecules or drugs such as bisphosphonates adsorbed on apatitic surfaces.[18]

In contrast, as reported by some authors, a fast release by a simple diffusion process can be observed from the pure polymeric matrix such as PEI,[37] which can completely release drugs by penetration of the liquid and chains swelling. Indeed, for ZnHAPEIBP composite support, the release kinetic reached a plateau within a few minutes (Figure 3b), which is in accordance also with the proposed Freundlich adsorption model. However, no more than 3% of the initial quantity of BP adsorbed on ZnHAPEIBP was released after 30 min, and no more release was observed at the end of 3 days, despite the relatively higher quantity of risedronate adsorbed on ZnHAPEIBP compared with ZnHABP. No difference in the specific surface area was observed between ZnHABP and ZnHAPEIBP that could explain such a low release. Thus, risedronate release from the ZnHAPEIBP support is not controlled by simple diffusion (r^2 = 0.24) as generally observed from pure polymeric matrix such as branched PEI,[37] or from PEI modified hydroxyapatite (HAPEI).[19] In particular, the small amount of BP release from ZnHAPEIBP in comparison to that previously reported for HAPEIBP[19] can be related to the different methods of preparation of the supports: adsorption from solution, utilized for the synthesis of ZnHAPEI, leads to a significantly higher polymer content (5.9 wt %) than coprecipitation (2.9 wt %) utilized for HAPEI.[19] The higher content of the polycationic polymer on ZnHAPEI compared with HAPEI should enhance interaction with the negatively charged risedronate, promoting BP adsorption and limiting BP release.

This short term release study was implemented to compare and model the first hours of risedronate release from the two apatitic supports, especially in order to study the influence of the presence of PEI, in a simple medium at pH 7.4 and 37 °C. Interestingly, no burst release was observed, which is a good point for the development of such apatitic local drug delivery systems able to have an effect on osteoclastogenesis and bone resorption.

In Vitro Tests. In vitro tests were performed on disk shaped samples, which were prepared by pressing the powders of the different materials. Cells response is greatly influenced by the topography of the samples.[38] Therefore, it is important to check and control the roughness of the surface of the samples prepared for in vitro tests. To this aim, surface

investigation of the disks was performed through AFM analysis (Figure 5). The results indicated similar values of roughness

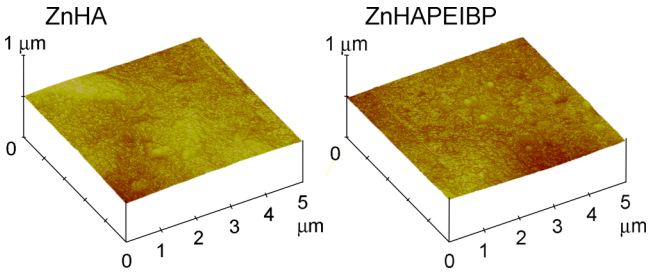


Figure 5. Atomic force microscopy images of the surfaces of disk shaped samples obtained by pressing as prepared ZnHA and ZnHAPEIBP powders into cylindrical molds and used for cell tests.

parameters, arithmetic mean roughness (Ra), root square roughness (Rq), and the vertical distance between the highest and lowest points within the evaluation length (Rt), for all tested samples. Indeed, the average values recorded are Ra = 0.017 ± 0.002 μm, Rq = 0.023 ± 0.002 μm, and Rt = 0.195 ± 0.008 μm for ZnHA disks (composed from the starting powders without further functionalization), and Ra = 0.025 ± 0.002 μm, Rq = 0.031 ± 0.003 μm, and Rt = 0.233 ± 0.013 μm for ZnHAPEIBP samples.

Cell Viability and Morphology. Oxidative stress is involved in numerous pathologies, including osteoporosis, because of its role in bone turnover. In this study cocultures were treated with 0.3 mM H_2O_2 for 48 h in order to study the effect of risedronate presence on cell behavior in an unfavorable microenvironment, simulating oxidative stress. Viability was studied at 3 and 7 days on experimental treated groups (ZnHA+, ZnHAPEI+, ZnHABP+, ZnHAPEIBP+) and compared to treated (HA+) and untreated (HA−, ZnHA−) reference groups and OB or OC monolayer without materials (CTR , CTR+). A significant difference in osteoblast viability after both 3 and 7 days of culture can be observed between treated groups CTR+, HA+, ZnHA+, ZnHAPEI+, ZnHA PEIBP+ and the reference group CTR−, HA−, ZnHA− (Table S2). On the contrary, osteoblast viability is significantly enhanced in the ZnHABP+ group (Figure 6) when compared to other treated groups, and ZnHAPEIBP+ when compared to ZnHA+, indicating that the presence of risedronate allows recovery of impairment due to the oxidative stress conditions created in vitro. Representative images of osteoblasts grown onto material samples, shown in Figure 6, confirm the optical density values obtained by the WST1 test.

Osteoclast viability on CTR, HA, and ZnHA both at 3 and 7 days does not differ significantly when treated (+) and untreated (−) groups were compared (Table S2, Figure 6), showing that H_2O_2 treatment does not affect osteoclast viability, in agreement with previous results.[39] At variance, the presence of PEI and/or BP significantly decreases osteoclast viability, suggesting an inhibitory role of both functionalizing agents.

Cell Activity. Bioactivity of cocultured osteoblasts was assessed by evaluation of the most common markers of osteoblast differentiation, by measuring both protein produc tion and gene expression. As shown in Figures 7a−c and S6, the results of the immunoenzymatic assays demonstrate that

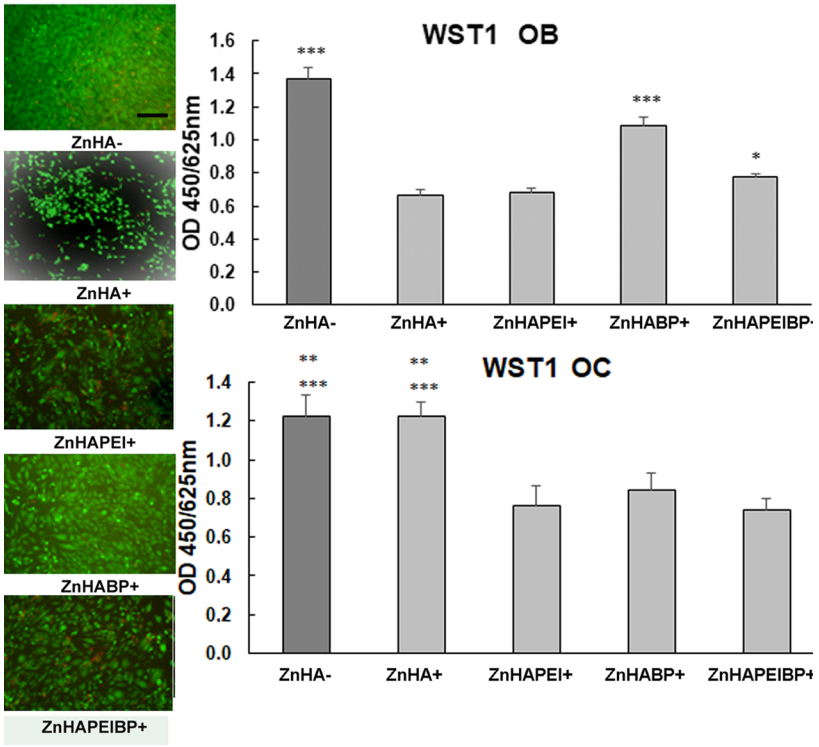


Figure 6. Osteoblast and osteoclast viability by the WST1 test after 7 days of coculture on material samples in oxidative stress environment (ZnHA +, ZnHAPEI+, ZnHABP+, ZnHAPEIBP+) and reference (ZnHA−). Statistical analysis is reported in the figure (*p < 0.05, **p < 0.005, ***p < 0.0005). Live & Dead staining of OB cultured onto samples. Images appeared consisting with WST1 values. Magnification in all the images is the same, bar = 200 μm. OB: ***ZnHA− vs ZnHA+, ZnHAPEI+, ZnHABP+, ZnHAPEIBP+; ***ZnHABP+ vs ZnHA+, ZnHAPEI+, ZnHAPEIBP+; * ZnHAPEIBP+ vs ZnHA+; OC: ***ZnHA−, ZnHA+ vs ZnHAPEI+, ZnHAPEIBP+; **ZnHA−, ZnHA+ vs ZnHABP+.

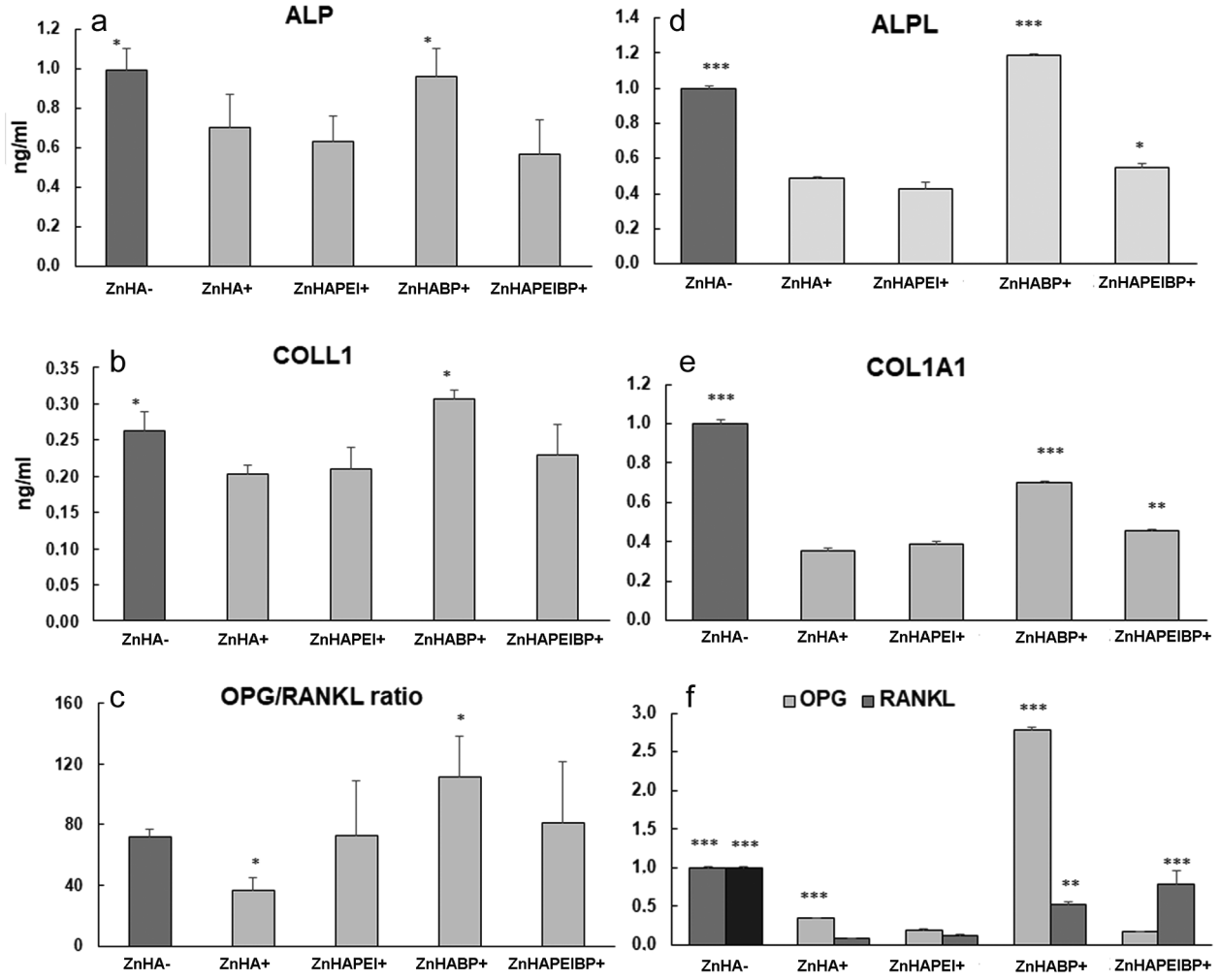


Figure 7. Immunoenzymatic assay on supernatant (a–c) and gene expression (d–f) of cocultured OB on material ZnHA+, ZnHAPEI+, ZnHABP +, and ZnHAPEIBP+ in oxidative stress conditions and reference (ZnHA–) after 7 days of incubation. ELISA tests data were normalized to WST1 values. Gene expression data were normalized to GAPDH expression and presented as fold change relative to the reference group, considered as 1. Results are the mean (± sd) of six replicates. Statistical analysis is reported in the figure (*$p < 0.05$, **$p < 0.005$, ***$p < 0.0005$). (a) ALP: *ZnHA–, ZnHABP+ vs ZnHA+, ZnHAPEI+, ZnHAPEIBP+. (b) COLL1: *ZnHA– vs ZnHA+; *ZnHABP+ vs ZnHA–, ZnHA+, ZnHAPEI+, ZnHAPEIBP+; (c) OPG/RANKL ratio: *ZnHABP+ vs ZnHA–; *ZnHA+ vs ZnHA–, ZnHABP+, ZnHAPEIBP+; (d) ALPL: ***ZnHABP+ vs ZnHA–, ZnHA+, ZnHAPEI+, ZnHAPEIBP+; ***ZnHA– vs ZnHA+, ZnHAPEI+, ZnHAPEIBP+; * ZnHAPEIBP+ vs ZnHAPEI+; (e) COL1A1: ***ZnHA– vs ZnHA+, ZnHAPEI+, ZnHABP+, ZnHAPEIBP+; ***ZnHABP+ vs ZnHA+, ZnHAPEI+, ZnHAPEIBP+; **ZnHAPEIBP+ vs ZnHA+, ZnHAPEI+; (f) OPG: ***ZnHABP+ vs ZnHA–, ZnHA+, ZnHAPEI+, ZnHAPEIBP+; ***ZnHA– vs ZnHA+, ZnHAPEI+, ZnHAPEIBP+; ***ZnHA+ vs ZnHAPEI+, ZnHAPEIBP+; RANKL: ***ZnHA– vs ZnHA+, ZnHAPEI+, ZnHABP+; **ZnHABP+ vs ZnHA+, ZnHAPEI+; ***ZnHAPEIBP+ vs ZnHA+, ZnHAPEI+.

the values of ALP, COLL1, and OPG produced by osteoblasts grown on ZnHA+ are significantly lower than those measured for ZnHA–. On the contrary, RANKL in the ZnHA+ group is significantly higher than in ZnHA–, causing a significant reduction of the OPG/RANKL ratio of ZnHA+ in comparison to ZnHA–. OPG and RANKL are expressed by osteoblasts and are known to be essential for regulating osteoclast differentiation.[40]

The impairment due to in vitro created oxidative stress is not recovered in the samples containing PEI, which show values of osteoblast differentiation markers similar to those measured for ZnHA+. On the contrary, the activity of OB is significantly improved in the presence of risedronate, so that it brings the activity of ZnHABP+ group back to the normal reference level: the measured values of ALP and OPG reach those obtained in the reference group ZnHA–, with no significant differences between ZnHABP+ and ZnHA–. COLL1 is significantly higher in ZnHABP+ than in all other groups, including the reference one, whereas the OPG/RANKL ratio assumes the highest value on ZnHABP+, which is significantly different for both ZnHA– and ZnHA+.

Therefore, risedronate stimulates the activity of the OB even in an unfavorable situation as in the presence of oxidative stress/aging, showing a behavior similar to that previously reported for alendronate.[39] The reduction of the negative effects of H_2O_2 on viability and activity of OB induced by risedronate in ZnHABP+ is less evident when PEI is also present on the sample surface: OB viability on ZnHAPEIBP+ is lower than on ZnHABP+, although higher than on ZnHA+, whereas ALP and COLL1 values on ZnHAPEIBP+ are not significantly different from those for ZnHA+.

The statistical evaluation of gene expression of the same parameters of OB activity measured by immunoenzymatic assays is consistent with the results shown above (Figure 7d–

f). The presence of risedronate increased ALPL and COL1A1 gene expression in both ZnHABP+ and, even if to a lesser amount, on ZnHAPEIBP+. Also OPG and RANKL expression demonstrated to be in line with immunoenzymatic assays, results showing in particular a significant higher expression of OPG for ZnHABP+ when compared to all other groups.

The less beneficial effect exerted by risedronate on osteoblast viability and differentiation in the PEI functionalized sample, ZnHAPEIBP, might be related to its reduced extent of release in comparison to that measured from ZnHABP (Figure 3b). In the examined conditions, the percentage of risedronate released from ZnHABP is more than twice that released from ZnHAPEIBP. Although the conditions utilized for measure ment of risedronate release profile were quite different from those of the cell culture environment, it is conceivable to hypothesize that also during in vitro experiments the amount of risedronate released from ZnHAPEIBP was less than from ZnHABP and possibly too small to allow complete recovery from the negative effects of H_2O_2 treatment on osteoblasts.

On the other hand, both PEI and risedronate affect osteoclast activity. The expression of cathepsin K (CTSK), which is secreted by active osteoclasts and is a promoter of bone resorption,[41] was measured in order to evaluate the degree of osteoclast differentiation. The results, reported in Figure 8, show that oxidative stress provokes an increase in the expression of CTSK, which reaches its highest level on ZnHA +. The level is slightly less on ZnHAPEI+, whereas it is significantly reduced on ZnHABP+ and ZnHAPEIBP+, in agreement with an inhibitory role of risedronate on osteoclast activity. Moreover, the results of TRAP staining show that osteoclast formation by monocytes is not affected by H_2O_2 treatment. TRAP staining displays a reduced value on ZnHAPEI+, indicating that PEI, in addition to significantly reducing the number of OC, also partially reduces OC differentiation. However, the major role is played by risedronate, which lowers both OC differentiation, as stated by the drastically reduced expression of CSTK and TRAP positive cells, and OC number, through a direct action on osteoclast viability as well as an osteoblast mediated regulation of OPG/RANKL pathway.

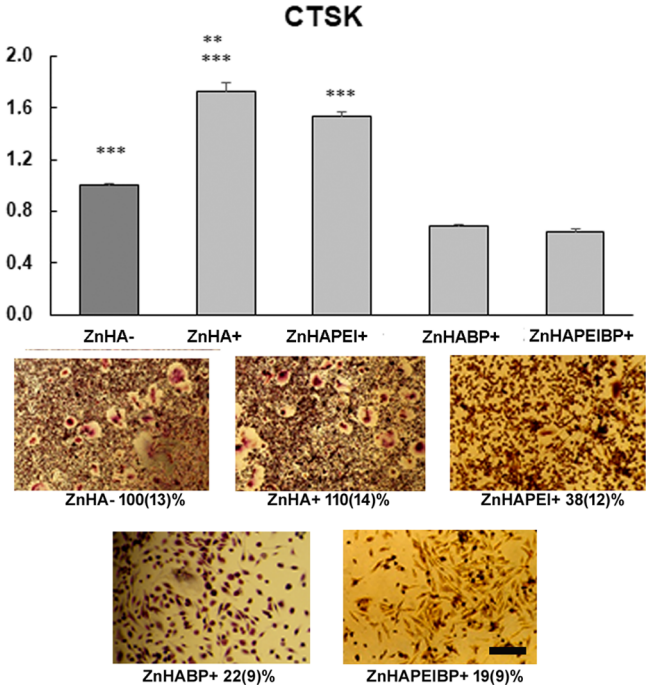


Figure 8. Gene expression of CTSK (a) and TRAP staining (b) of cocultured OC on material ZnHA+, ZnHAPEI+, ZnHABP+, and ZnHAPEIBP+ in oxidative stress conditions and reference (ZnHA−) after 7 days of incubation. The expression of CTSK was normalized to GAPDH expression and presented as fold change relative to the ZnHA− reference group, considered as 1. Results are the mean (± sd) of six replicates. Statistical analysis is reported in the figure (*p < 0.05, **p < 0.005, ***p < 0.0005). Differentiated OC after TRAP staining were quantified by counting the number of TRAP positive cells in six fields each group, under the microscope (4×) by a semiautomatic software (NIS Elements AR 4.30.01), and the percentage is reported in the figure, considering ZnHA− as a reference (100%). Magnification in all the images is the same, bar = 200 μm. CTSK: ***ZnHA+, ZnHAPEI+ vs ZnHA−, ZnHABP+, ZnHAPEIBP+; **ZnHA+ vs ZnHAPEI+; ***ZnHA− vs ZnHAPEI +, ZnHABP+. TRAP: *** ZnHA−, ZnHA+ vs ZnHAPEI+, ZnHABP +, ZnHAPEIBP+.

CONCLUSIONS

The bifunctionalized hydroxyapatite obtained in this work contains about 8 atom % of zinc substituted to calcium ions and about 5.9 wt % PEI loaded on the nanocrystals surface. The presence of PEI does not alter the structural and morphological characteristics of ZnHA but significantly increases the value of the zeta potential and promotes risedronate adsorption. In fact, the amount of adsorbed risedronate is higher on ZnHAPEIBP than on ZnHABP. The isotherm of the bisphosphonate adsorption on ZnHAPEI can be fitted with the Freundlich model (r^2 = 0.81), at variance with the adsorption on ZnHA which follows a Langmuir type isotherm (r^2 = 0.94). Moreover, phosphate release in solution from the ZnHAPEI support is not affected by the amount of adsorbed risedronate, suggesting that the mechanism of adsorption on ZnHAPEI is different from that described in the literature as an ion exchange process between phosphates on the apatitic surface and bisphosphonate in solution.[17,18] The strong interactions between the polycationic polymer and the negatively charged bisphosphonate can explain the much smaller quantity of risedronate released from ZnHAPEIBP than from ZnHABP. Both materials exhibit slow risedronate release profiles as required for antiresorptive bone substitute materials involving local and sustained drug delivery.

The results of in vitro cell tests carried out using a coculture model reveal a novel characteristic of risedronate: the data obtained on the differently functionalized samples indicate that risedronate presence counteracts the negative effects of H_2O_2, which is added to the culture medium to simulate conditions of oxidative stress, and enhances osteoblast viability and activity. The beneficial effect of risedronate on osteoblasts is slightly reduced in the PEI containing samples (ZnHAPEIBP). However, PEI contributes to lower osteoclast number and differentiation, as shown by CTSK and TRAP staining results. It follows that the best choice for local applications aimed to downregulate the excessive resorption activity of osteoclasts and/or to protect osteoblasts from an undesired increase of reactive oxygen species can be ZnHAPEIBP or ZnHABP, depending on the kinetics of bone metabolism.

■ ASSOCIATED CONTENT

● Supporting Information

The Supporting Information is available free of charge on the ACS Publications website at DOI: 10.1021/acsbiomaterials.9b00795.

Additional information for scheme of the molecular structures of risedronate and PEI; scheme of cellular seeding for in vitro model; thermogravimetric plot; TEM images of the supports; Raman spectra; X ray diffraction patterns; OPG and RANKL graphics; table with specifications of primer used for qPCR analysis, table with viability of monolayer (CTR) and HA in normal and under H_2O_2 conditions compared with experimental groups, at 3 and 7 days (PDF)

■ AUTHOR INFORMATION

Corresponding Author

*E mail: elisa.boanini@unibo.it.

ORCID

Christèle Combes: 0000 0001 5009 1973

Elisa Boanini: 0000 0003 3754 0273

Notes

The authors declare no competing financial interest.

■ ACKNOWLEDGMENTS

The authors thank the European MP 1301 COST action (New Generation Biomimetic and Customized Implants for Bone Engineering (NEWGEN); 2013 2017), the University of Bologna (Marco Polo program 2016), and Rizzoli Orthopaedic Institute (funds 5x1000 year 2016, cod. 7162) for supporting this bilateral research work.

■ REFERENCES

(1) Shahar, R.; Weiner, S. Open Questions on the 3D Structures of Collagen Containing Vertebrate Mineralized Tissues: A Perspective. *J. Struct. Biol.* 2018, *201*, 187−198.

(2) Glimcher, M. J. Bone: Nature of the Calcium Phosphate Crystals and Cellular, Structural, and Physical Chemical Mechanisms in Their Formation. *Rev. Mineral. Geochem.* 2006, *64*, 223−282.

(3) Bigi, A.; Boanini, E.; Gazzano, M. Ion Substitution in Biological and Synthetic Apatites. In *Biomineralization and Biomaterials, Foundamentals and Applications*; Aparicio, C.; Ginebra, M. P., Eds.; Woodhead Publishing (Imprint Elsevier): Cambridge, UK, 2015; pp 235−266. DOI: DOI: 10.1016/B978 1 78242 338 6.00008 9.

(4) Ridi, F.; Meazzini, I.; Castroflorio, B.; Bonini, M.; Berti, D.; Baglioni, P. Functional Calcium Phosphate Composites in Nano medicine. *Adv. Colloid Interface Sci.* 2017, *244*, 281−295.

(5) Bigi, A.; Boanini, E. Functionalized Biomimetic Calcium Phosphates for Bone Tissue Repair. *J. Appl. Biomater. Funct. Mater.* 2017, *15*, e313−e325.

(6) Verron, E.; Schmid Antomarchi, H.; Pascal Mousselard, H.; Schmid Alliana, A.; Scimeca, J. C.; Bouler, J. M. Therapeutic Strategies for Treating Osteolytic Bone Metastases. *Drug Discovery Today* 2014, *19*, 1419−1426.

(7) Bigi, A.; Boanini, E. Calcium Phosphates as Delivery Systems for Bisphosphonates. *J. Funct. Biomater.* 2018, *9* (6). DOI: DOI: 10.3390/jfb9010006.

(8) Russell, R. G. G. Bisphosphonates: the First 40 Years. *Bone* 2011, *49*, 2−19.

(9) Giger, E. V.; Castagner, B.; Leroux, J. C. Biomedical Applications of Bisphosphonates. *J. Controlled Release* 2013, *167*, 175−188.

(10) Fazil, M.; Baboota, S.; Sahni, J. K.; Ameeduzzafar; Ali, J. Bisphosphonates: Therapeutics Potential and Recent Advances in Drug Delivery. *Drug Delivery* 2015, *22*, 1−9.

(11) Verron, E.; Bouler, J. M. Is Bisphosphonate Therapy Compromised by the Emergence of Adverse Bone Disorders? *Drug Discovery Today* 2014, *19*, 312−319.

(12) Favia, G.; Pilolli, G. P.; Maiorano, E. Histologic and Histomorphometric Features of Bisphosphonate Related Osteonec rosis of the Jaws: an Analysis of 31 Cases with Confocal Laser Scanning Microscopy. *Bone* 2009, *45*, 406−413.

(13) Rizzoli, R.; Åkesson, K.; Bouxsein, M.; Kanis, J. A.; Napoli, N.; Papapoulos, S.; Reginster, J. Y.; Cooper, C. Subtrochanteric Fractures After Long Term Treatment with Bisphosphonates: a European Society on Clinical and Economic Aspects of Osteoporosis and Osteoarthritis, and International Osteoporosis Foundation Working Group Report. *Osteoporosis Int.* 2011, *22*, 373−390.

(14) McClung, M. Bisphosphonates. *Arq. Bras. Endocrinol. Metabol.* 2006, *50*, 735−744.

(15) Nancollas, G. H.; Tang, R.; Phipps, R. J.; Henneman, Z.; Gulde, S.; Wu, W.; Mangood, A.; Russell, R. G.; Ebetino, F. H. Novel Insights into Actions of Bisphosphonates on Bone: Differences in Interactions with Hydroxyapatite. *Bone* 2006, *38*, 617−627.

(16) Errassifi, F.; Sarda, S.; Barroug, A.; Legrouri, A.; Sfihi, H.; Rey, C. Infrared, Raman and NMR Investigations of Risedronate Adsorption on Nanocrystalline Apatites. *J. Colloid Interface Sci.* 2014, *420*, 101−111.

(17) Al Kattan, A.; Errassifi, F.; Sautereau, A. M.; Sarda, S.; Dufour, P.; Barroug, A.; Dos Santos, I.; Combes, C.; Grossin, D.; Rey, C.; Drouet, C. Medical Potentialities of Biomimetic Apatites through Adsorption, Ionic Substitution, and Mineral/Organic Associations: Three Illustrative Examples. *Adv. Eng. Mater.* 2010, *12* (7), B224−B233.

(18) Pascaud, P.; Errassifi, F.; Brouillet, F.; Sarda, S.; Barroug, A.; Legrouri, A.; Rey, C. Adsorption on Apatitic Calcium Phosphates for Drug Delivery: Interaction with Bisphosphonate Molecules. *J. Mater. Sci.: Mater. Med.* 2014, *25*, 2373−2381.

(19) Forte, L.; Sarda, S.; Combes, C.; Brouillet, F.; Gazzano, M.; Marsan, O.; Boanini, E.; Bigi, A. Hydroxyapatite Functionalization to Trigger Adsorption and Release of Risedronate. *Colloids Surf., B* 2017, *160*, 493−499.

(20) Shepherd, D. V.; Kauppinen, K.; Brooks, R. A.; Best, S. M. An *In Vitro* Study into the Effect of Zinc Substituted Hydroxyapatite on Osteoclast Number and Activity. *J. Biomed. Mater. Res., Part A* 2014, *102*, 4136−4141.

(21) Yamada, Y.; Ito, A.; Kojima, H.; Sakane, M.; Miyakawa, S.; Uemura, T.; LeGeros, R. Z. Inhibitory Effect of Zn^{2+} in Zinc Containing Beta Tricalcium Phosphate on Resorbing Activity of Mature Osteoclasts. *J. Biomed. Mater. Res. Part A* 2008, *84A*, 344−352.

(22) Wang, X. P.; Ito, A.; Sogo, Y.; Li, X.; Oyane, A. Zinc Containing Apatite Layers on External Fixation Rods Promoting Cell Activity. *Acta Biomater.* 2010, *6*, 962−968.

(23) Li, X.; Sogo, Y.; Ito, A.; Mutsuzaki, H.; Ochiai, N.; Kobayashi, T.; Nakamura, S.; Yamashita, K.; LeGeros, R. Z. The Optimum Zinc Content in Set Calcium Phosphate Cement for Promoting Bone Formation in Vivo. *Mater. Sci. Eng., C* 2009, *29*, 969−975.

(24) Kwak, H. B.; Kim, J. Y.; Kim, K. J.; Choi, M. K.; Kim, J. J.; Kim, K. M.; Shin, Y. I.; Lee, M. S.; Kim, H. S.; Kim, J. W.; Chun, C. H.; Cho, H. J.; Hong, G. Y.; Juhng, S. K.; Yoon, K. H.; Park, B. H.; Bae, J. M.; Han, J. K.; Oh, J. Risedronate Directly Inhibits Osteoclast Differentiation and Inflammatory Bone Loss. *Biol. Pharm. Bull.* 2009, *32*, 1193−1198.

(25) D'Amelio, P.; Grimaldi, A.; Di Bella, S.; Tamone, C.; Brianza, S. Z.; Ravazzoli, M. G.; Bernabei, P.; Cristofaro, M. A.; Pescarmona, G. P.; Isaia, G. Risedronate Reduces Osteoclast Precursors and Cytokine Production in Postmenopausal Osteoporotic Women. *J. Bone Miner. Res.* 2008, *23*, 373−379.

(26) Ren, F.; Xin, R.; Ge, X.; Leng, Y. Characterization and Structural Analysis of Zinc Substituted Hydroxyapatites. *Acta Biomater.* 2009, *5*, 3141−3149.

(27) Fuierer, T. A.; LoRe, M.; Puckett, S. A.; Nancollas, G. H. A Mineralization Adsorption and Mobility Study of Hydroxyapatite

Surfaces in the Presence of Zinc and Magnesium Ions. *Langmuir* **1994**, *10*, 4721−4725.
(28) Bigi, A.; Foresti, E.; Gandolfi, M.; Gazzano, M.; Roveri, N. Inhibiting Effect of Zinc on Hydroxylapatite Crystallization. *J. Inorg. Biochem.* **1995**, *58*, 49−58.
(29) Thomas, M.; Ge, Q.; Lu, J. J.; Chen, J.; Klibanov, A. M. Cross Linked Small Polyethylenimines: While Still Nontoxic, Deliver DNA Efficiently to Mammalian Cells In Vitro and In Vivo. *Pharm. Res.* **2005**, *22*, 373−380.
(30) Boanini, E.; Torricelli, P.; Bonvicini, F.; Cassani, M. C.; Fini, M.; Gentilomi, G. A.; Bigi, A. A New Multifunctionalized Material Against Multi Drug Resistant Bacteria and Abnormal Osteoclast Activity. *Eur. J. Pharm. Biopharm.* **2018**, *127*, 120−129.
(31) Bigi, A.; Boanini, E.; Cojazzi, G.; Falini, G.; Panzavolta, S. Morphological and Structural Investigation of Octacalcium Phosphate Hydrolysis in Presence of Polyacrylic Acids: Effect of Relative Molecular Weights. *Cryst. Growth Des.* **2001**, *1*, 239−244.
(32) Eichert, D.; Drouet, C.; Sfihi, H.; Rey, C.; Combes, C. Nanocrystalline Apatite Based Biomaterials: Synthesis Processing and Characterization. In *Biomaterials Research Advances*; Kendall, J. B., Ed.; Nova Science Publishers: New York, 2008; pp 93−143.
(33) Sanchez Cortes, S.; Berenguel, R. M.; Madejon, A.; Perez Mendez, M. Adsorption of Polyethyleneimine on Silver Nanoparticles and its Interaction with a Plasmid DNA: a Surface Enhanced Raman Scattering Study. *Biomacromolecules* **2002**, *3*, 655−660.
(34) Gao, B.; Jiang, P.; Lei, H. Studies on Adsorption Property of Novel Composite Adsorption Material PEI/SiO_2 for Uric Acid. *Mater. Lett.* **2006**, *60*, 3398−3404.
(35) Cukrowski, I.; Popovic, L.; Barnard, W.; Paul, S. O.; van Rooyen, P. H.; Liles, D. C. Modeling and Spectroscopic Studies of Bisphosphonate Bone Interactions. The Raman, NMR and Crystallo graphic Investigations of Ca HEDP Complexes. *Bone* **2007**, *41*, 668−678.
(36) Costa, P.; Sousa Lobo, J. M. Modeling and Comparison of Dissolution Profiles. *Eur. J. Pharm. Sci.* **2001**, *13*, 123−133.
(37) Demadis, K. D.; Paspalaki, M.; Theodorou, J. Controlled Release of Bis (Phosphonate) Pharmaceuticals from Cationic Biodegradable Polymeric Matrices. *Ind. Eng. Chem. Res.* **2011**, *50*, 5873−5876.
(38) Fini, M.; Giardino, R.; Borsari, V.; Torricelli, P.; Rimondini, L.; Giavaresi, G.; Aldini, N. N. *In Vitro* Behaviour of Osteoblasts Cultured on Orthopaedic Biomaterials with Different Surface Roughness, Uncoated and fluorohydroxyapatite coated, relative to the *in Vivo* Osteointegration Rate. *Int. J. Artif. Organs* **2003**, *26*, 520−528.
(39) Forte, L.; Torricelli, P.; Boanini, E.; Rubini, K.; Fini, M.; Bigi, A. Quercetin and Alendronate Multi Functionalized Materials as Tools to Hinder Oxidative Stress Damage. *J. Biomed. Mater. Res., Part A* **2017**, *105A*, 3293−3303.
(40) Katagiri, T.; Takahashi, N. Regulatory Mechanisms of Osteoblast and Osteoclast Differentiation. *Oral Dis.* **2002**, *8*, 147−159.
(41) Hemingway, F.; Cheng, X.; Knowles, H. J.; Estrada, F. M.; Gordon, S.; Athanasou, N. A. In Vitro Generation of Mature Human Osteoclasts. *Calcif. Tissue Int.* **2011**, *89*, 389−395.

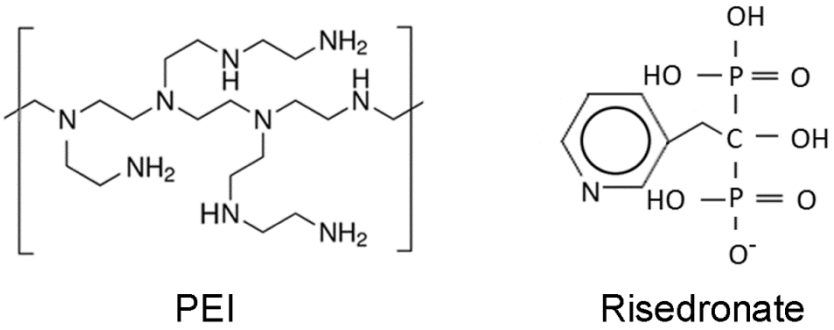
Supplementary Information

Multi-functionalization modulates hydroxyapatite surface interaction with bisphosphonate: anti-osteoporotic and antioxidative stress materials.

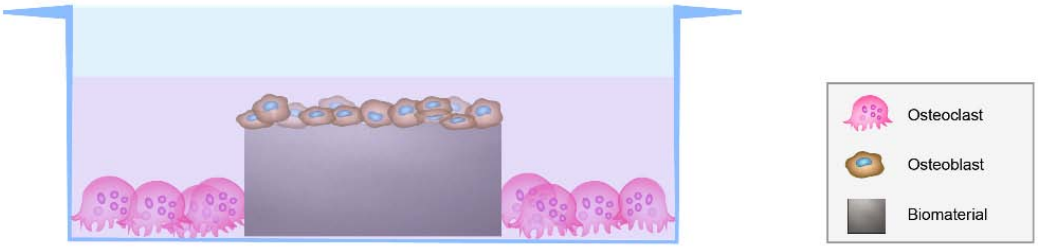
Lucia Forte, Stéphanie Sarda, Paola Torricelli, Christèle Combes, Fabien Brouillet, Olivier Marsan, Francesca Salamanna, Milena Fini, Elisa Boanini, Adriana Bigi

Content:

- Scheme S1
- Scheme S2
- Figures from S1 to S6
- Table S1
- Table S2



Scheme S1. Molecular structures of polyethylenimine (PEI) and risedronate.



Scheme S2. Scheme of cell seeding for the co-culture model

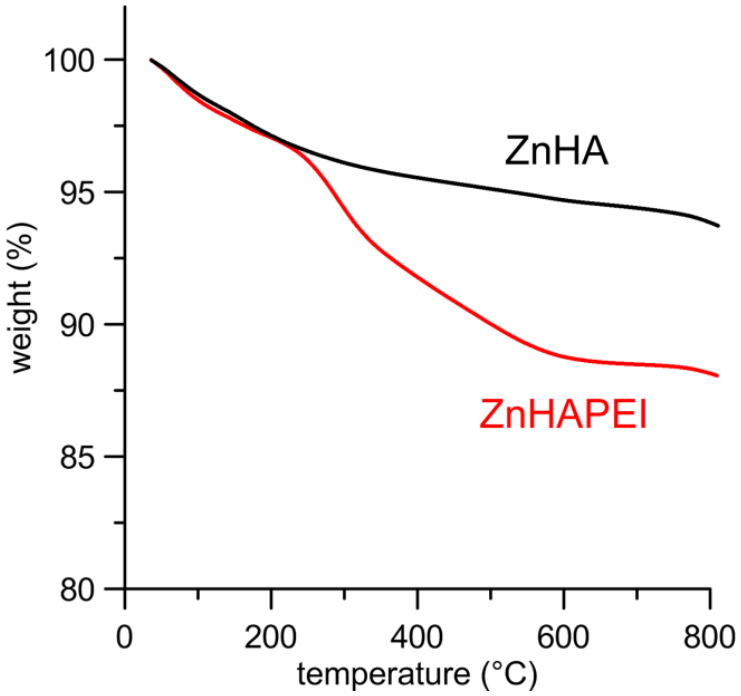


Figure S1 – Thermogravimetric plot of ZnHA and ZnHAPEI. The weight loss centered at about 400°C is due to the combustion of organic fraction and allows to determine that ZnHAPEI sample contains about 5.9 wt% PEI.

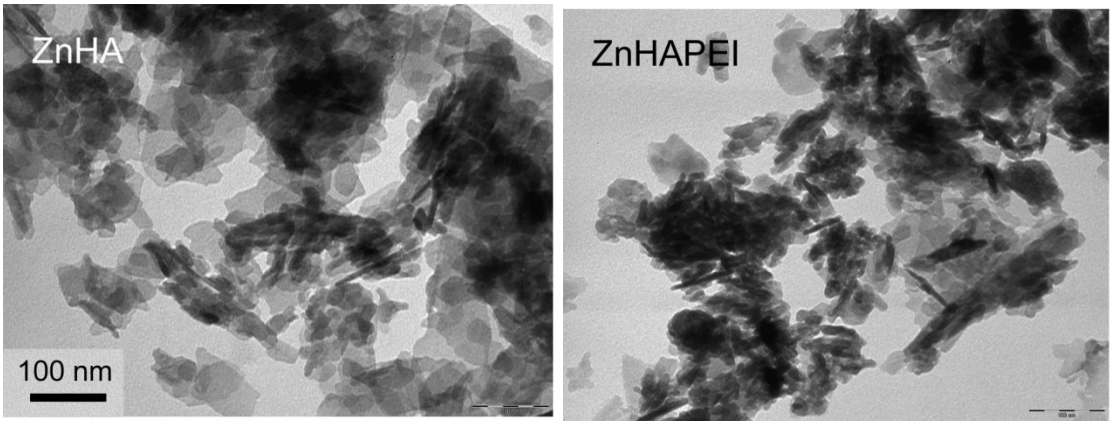


Figure S2 – TEM images of the supports ZnHA and ZnHAPEI before risedronate adsorption. Magnification in all TEM images is the same for direct comparison.

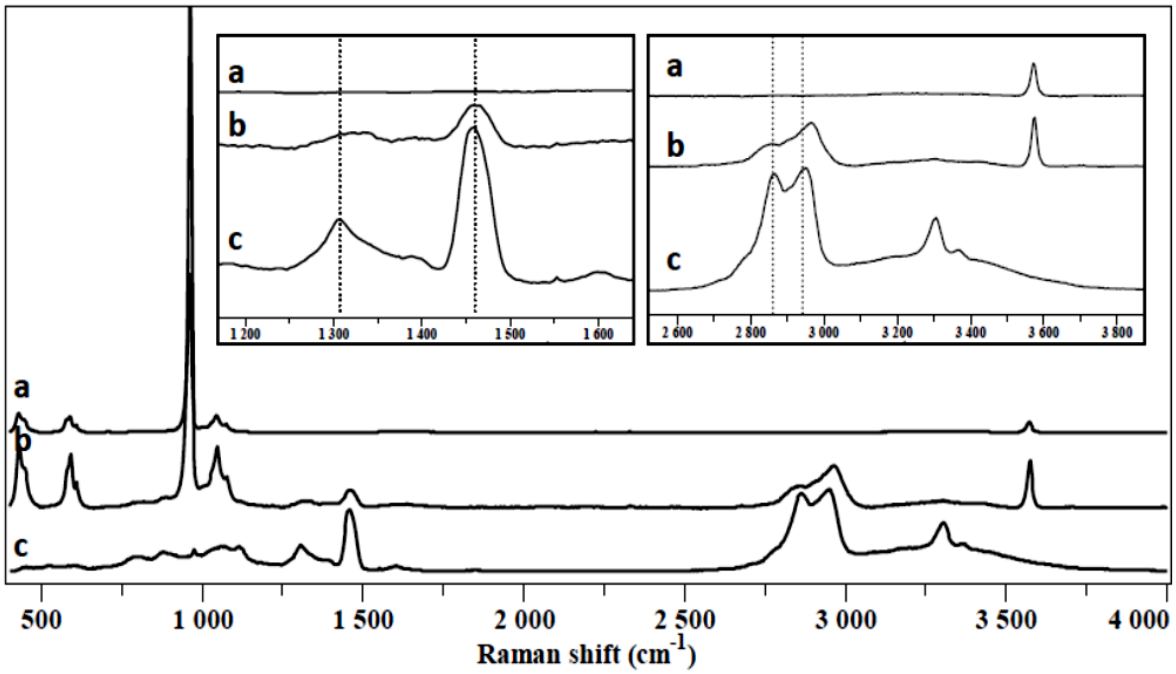


Figure S3 – Raman spectra of ZnHA (a), ZnHAPEI (b), PEI (c). The two insets focus on two spectral domains (1150-1650 cm^{-1} and 2550-3850 cm^{-1}) showing especially the main characteristic vibration bands for CH and CH_2 groups in PEI molecule.

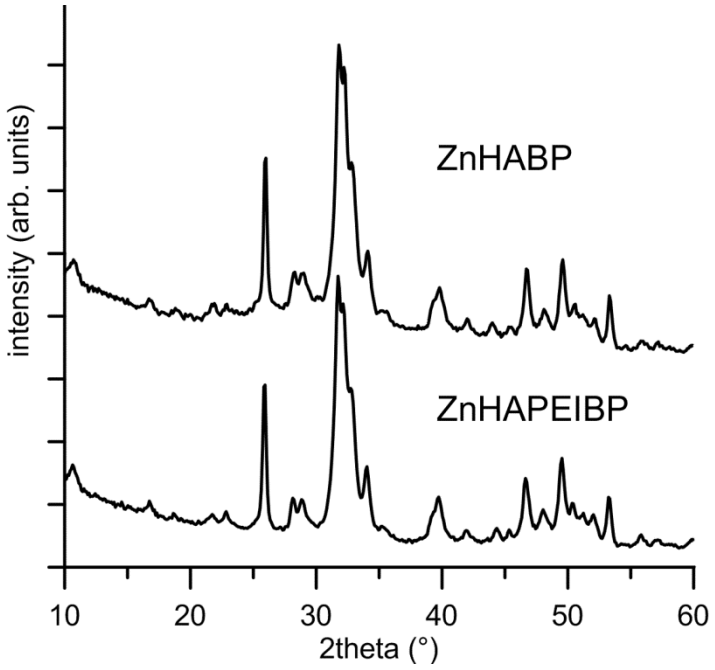


Figure S4 – X-ray diffraction patterns of ZnHABP and ZnHAPEIBP. The adsorption of risedronate does not alter the crystallinity of pristine apatitic substrates and does not provoke precipitation of any other crystalline phase.

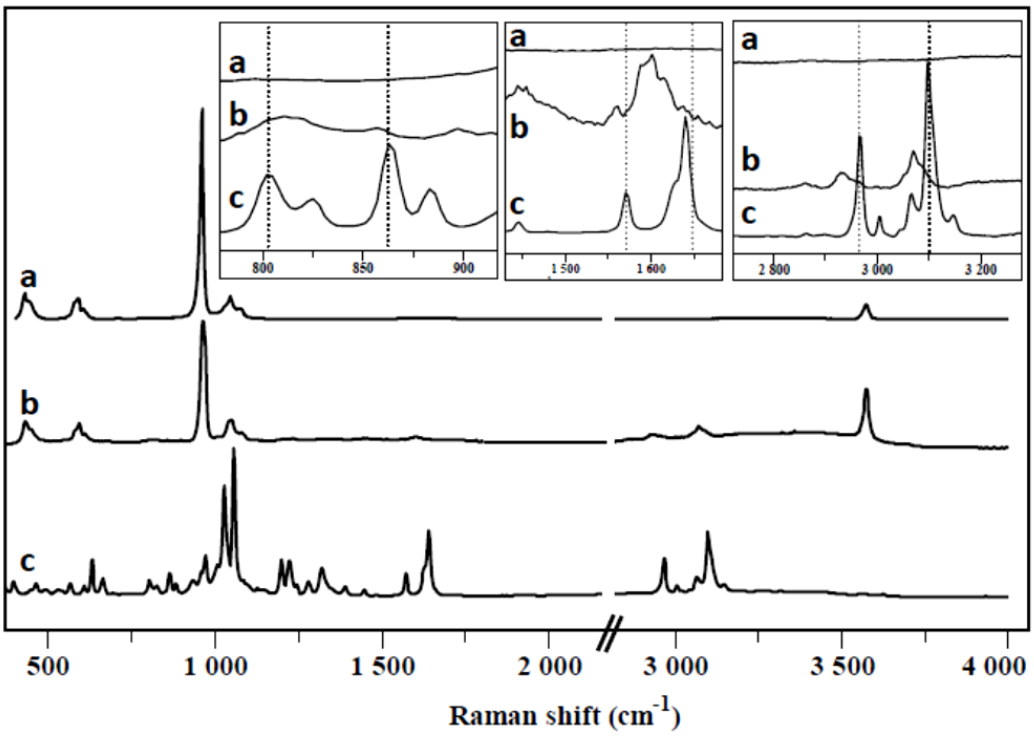


Figure S5 – Raman spectra of ZnHA (a), ZnHABP (b), risedronate (BP) sodium salt (c). The insets focus each on a spectral domain (775-925 cm^{-1}, 1375-1675 cm^{-1} and 2700-3300 cm^{-1}) to show the main characteristic vibration bands of risedronate molecule (pyridine ring, phosphonate group, C-H, C=C and C=N groups).

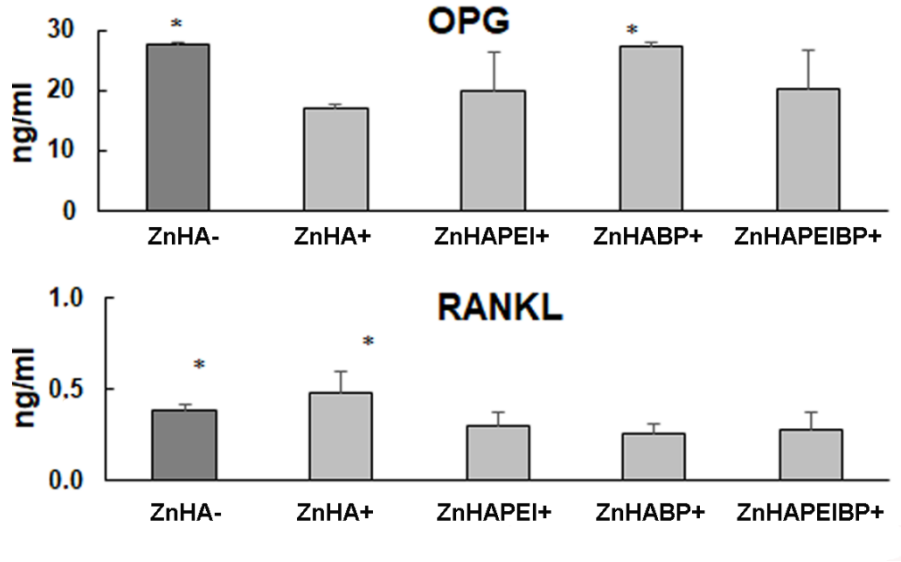


Figure S6 – OPG and RANKL levels on supernatant of ZnHA+, ZnHAPEI+, ZnHABP+, ZnHAPEIBP+ materials cultured with osteoblasts and osteoclasts in oxidative stress conditions and reference (ZnHA-) after 7 days of incubation. Statistical analysis is reported in the figure (*$p < 0.05$).

OPG: *ZnHA-, ZnHABP+ vs ZnHA+, ZnHAPEI+, ZnHAPEIBP+;

RANKL: *ZnHA- vs ZnHAPEI+, ZnHABP+; *ZnHA+ vs ZnHAPEI+, ZnHABP+, ZnHAPEIBP+.

Table S1. Specifications of primer used for qPCR analysis.

GENE	Primer forward	Primer reverse	Amplicon Lenght	Annealing Temperature
GAPDH	5'-TGGTATCGTGGAAGGACTCA-3'	5'-GCAGGGATGATGTTCTGGA -3'	123 bp	56°C
ALPL	QuantiTect Primer Assay (Qiagen) Hs_ALPL_1_SG		110 bp	55°C
COL1A1	QuantiTect Primer Assay (Qiagen) Hs_COL1A1_1_SG		118 bp	55°C
CTSK	CAGACAACAGATTTCCATCAGC	CTTCTTCCATAGCTCCCAGTG	118 bp	60°C
OPG	CTACCAAGACACTAAGCCAGT	AAACAGTGAATCAACTCAAAAATGTG	113 bp	60°C
RANKL	TGAGATGAGCAAAAGGCTGAG	AGGAGCTGTGCAAAAGGAAT	134 bp	60°C

Table S2. Viability of monolayer (CTR) and HA in normal (-) and under H_2O_2 (+) conditions together with other experimental groups at 3 and 7 days.

Group	WST1 assay			
	OB 3 days	OB 7 days	OC 3 days	OC 7 days
CTR-	0.917+/-0.028	1.315+/-0.200	1.248+/-0.035	1.248+/-0.035
HA-	0.807+/-0.039	1.262+/-0.018	1.281+/-0.078	1.279+/-0.023
ZnHA-	0.838+/-0.048	1.368+/-0.067	1.255+/-0.036	1.227+/-0.104
CTR+	0.539+/-0.047[a]	0.678+/-0.041[a]	1.254+/-0.032	1.254+/-0.032
HA+	0.478+/-0.046[a]	0.585+/-0.016[a]	1.255+/-0.007	1.269+/-0.037
ZnHA+	0.585+/-0.024[a]	0.662+/-0.036[a]	1.200+/-0.048	1.222+/-0.076
ZnHAPEI+	0.559+/-0.023[a]	0.679+/-0.031[a]	0.840+/-0.056[b]	0.761+/-0.102[b]
ZnHABP+	0.773+/-0.033	1.085+/-0.054	0.821+/-0.023[b]	0.843+/-0.092[b]
ZnHAPEIBP+	0.641+/-0.019[a]	0.780+/-0.017[a]	0.753+/-0.031[b]	0.739+/-0.063[b]

OB 3 and 7 days :

[a] CTR+, HA+, ZnHA+, ZnHAPEI+, ZnHAPEIBP+ vs CTR-, HA-, ZnHA-, ZnHABP+ ($p<0.0005$)

OC 3 and 7 days :

[b] ZnHAPEI+, ZnHABP+, ZnHAPEIBP+ vs all other groups ($p<0.0005$)